Received: 7 November 2017 | Revised: 9 February 2018 | Accepted: 10 February 2018

DOI: 10.1002/hbm.24011

RESEARCH ARTICLE

WILEY

The impact of B_1^+ correction on MP2RAGE cortical T_1 and apparent cortical thickness at 7T

Roy A.M. Haast[1,2] | Dimo Ivanov[1] | Kâmil Uludağ[1]

[1]Department of Cognitive Neuroscience, Faculty of Psychology and Neuroscience, Maastricht University, Maastricht, Netherlands

[2]Maastricht Centre for Systems Biology, Maastricht University, Maastricht, Netherlands

Correspondence
Roy A.M. Haast, Department of Cognitive Neuroscience, Faculty of Psychology & Neuroscience, Maastricht University, PO Box 616, 6200MD Maastricht, The Netherlands.
Email: roy.haast@maastrichtuniversity.nl

Funding information
Maastricht University; Netherlands Organization for Scientific Research (NWO), Grant/Award Number: 452-11-002; Technology Foundation STW, Grant/Award Number: 12724

Abstract

Determination of cortical thickness using MRI has often been criticized due to the presence of various error sources. Specifically, anatomical MRI relying on T_1 contrast may be unreliable due to spatially variable image contrast between gray matter (GM), white matter (WM) and cerebrospinal fluid (CSF). Especially at ultra-high field ($\geq$ 7T) MRI, transmit and receive B_1-related image inhomogeneities can hamper correct classification of tissue types. In the current paper, we demonstrate that residual B_1^+ (transmit) inhomogeneities in the T_1-weighted and quantitative T_1 images using the MP2RAGE sequence at 7T lead to biases in cortical thickness measurements. As expected, *post-hoc* correction for the spatially varying B_1^+ profile reduced the apparent T_1 values across the cortex in regions with low B_1^+, and slightly increased apparent T_1 in regions with high B_1^+. As a result, improved contrast-to-noise ratio both at the GM-CSF and GM-WM boundaries can be observed leading to more accurate surface reconstructions and cortical thickness estimates. Overall, the changes in cortical thickness ranged between a 5% decrease to a 70% increase after B_1^+ correction, reducing the variance of cortical thickness values across the brain dramatically and increasing the comparability with normative data. More specifically, the cortical thickness estimates increased in regions characterized by a strong decrease of apparent T_1 after B_1^+ correction in regions with low B_1^+ due to improved detection of the pial surface. The current results suggest that cortical thickness can be more accurately determined using MP2RAGE data at 7T if B_1^+ inhomogeneities are accounted for.

KEYWORDS
7T MRI, cortical thickness, MP2RAGE, quantitative T_1, transmit bias field

1 | INTRODUCTION

Segmentation of anatomical MRI data is considered as the *in vivo* gold standard for parcellating the brain into gray (GM) and white matter (WM). T_1-weighted (T_1w) images are predominantly used due to their high sensitivity to myelin concentration and, hence, high contrast between the cerebral spinal fluid (CSF, very low intensity), GM (medium intensity), and myelin-rich WM tissue (high intensity). Subsequent morphometric analyses of these tissue classes, including cortical GM thickness or subcortical GM and WM volume, allow characterization of cross-sectional differences between groups or longitudinal changes due to aging and disease. However, determination of cortical thickness based on MRI data has been criticized. The variation of myelin density across the cortical mantle, but also errors in T_1 quantification or MRI acquisition biases can result in reduced contrast between GM, WM, and CSF and, as a result, in inaccurate determination of cortical thickness (Han et al., 2006; Zilles & Amunts, 2015). Several software packages, for example, FreeSurfer (Dale, Fischl, & Sereno, 1999), FMRIB's software library (FSL; Smith et al., 2004), Statistical Parametric Mapping (SPM; Ashburner, 2009), and CBS High-Res Brain Processing tools (Bazin et al., 2014), have been developed to automatically classify different tissue classes based on image-

specific criteria using varying segmentation algorithms, hereby putting a large emphasis on bias field removal. In addition, many of these packages allow incorporation of complementary MRI data, such as $T_2^{(*)}$- or proton density (PD)-weighted images, to improve the accuracy of the (i.e., multimodal) segmentation algorithm by identifying nonbrain tissue, for example, dura mater and blood vessels (Helms, Kallenberg, & Dechent, 2006; Lambert, Lutti, Helms, Frackowiak, & Ashburner, 2013; Viviani et al., 2017).

Although the majority of, in particular clinical, neuroimaging data is acquired at 1.5T or 3T magnetic field strengths, technical developments and increased availability have led to increased usage of ultra-high-field scanners (UHF, $\geq$7T) for neuroanatomical and functional studies (as recently reviewed by De Martino et al., 2017; Marques & Norris, 2017; and Ugurbil, 2017, and references herein). Compared to conventional field strengths, imaging at higher fields enables acquisition of higher signal-to-noise ratio (SNR; Pohmann, Speck, & Scheffler, 2016) data and increases in various contrasts with no or little acquisition duration penalty. The increased SNR can be utilized to acquire data with higher spatial resolution, potentially leading to reduced partial volume effects (PVE) and, hence, more precise cortical GM thickness measurements. However, technical challenges remain in ensuring high image quality across the entire field-of-view. In particular, inhomogeneous radiofrequency (RF) B_1 transmit and receive profiles lead to signal intensity variations (i.e., B_1^+ and B_1^- bias fields, respectively) that hamper accurate classification of WM, GM, and CSF and cortical GM thickness estimates (Collins, Liu, Schreiber, Yang, & Smith, 2005; De Martino et al., 2015; Lorio et al., 2016; Van de Moortele et al., 2005). Especially for submillimeter acquisitions, laborious manual work is required to correct errors of the automatic segmentation, potentially introducing observer-dependent errors and biases (Despotovic, Goossens, & Philips, 2015; Fischl et al., 2004; Gulban, Schneider, Marquardt, Haast, & De Martino, 2018; Polimeni, Renvall, Zaretskaya, & Fischl, 2017). The most severe artefacts are observed toward the inferior temporal and frontal lobe regions, preventing even their manual segmentation.

Alternatively, in contrast to typically utilized *weighted* T_1 approaches, such as the Magnetization-Prepared Rapid Acquisition Gradient Echo (MPRAGE) sequence (Mugler & Brookeman, 1990), *quantitative* T_1 mapping can be used to obtain homogeneous images and accurate cortical thickness measurements by minimizing the contribution of B_1^+ and B_1^- variations, and PD and T_2* effects on the image intensities (Lorio et al., 2016). The inversion recovery (IR) method is considered to be the most accurate approach to determine T_1 values, as it acquires multiple time points in the longitudinal magnetization recovery curve after a 180° inversion. However, the main disadvantage of this method is its temporal inefficiency. Thus, alternative approaches have been proposed to reduce scanning duration and spatial distortions (which occur when the IR approach is combined with an EPI readout to decrease scanning time), while permitting accurate T_1 determination with satisfactory spatial resolution and SNR. These include, for example, spoiled gradient echo approaches, as implemented in several methods (Deoni, Rutt, & Peters, 2003; Helms, Dathe, & Dechent, 2008) or variations of the MPRAGE sequence (Liu, Bock, & Silva, 2011; Marques, Khabipova, & Gruetter, 2010). Here, the Magnetization-Prepared 2 Rapid Acquisition Gradient Echo (MP2RAGE) sequence has recently gained popularity in higher field strengths studies (Marques et al., 2010). It combines two gradient-recalled echo (GRE) images acquired at different inversion times (i.e., a predominantly T_1w GRE_1 and PDw GRE_2) to obtain a quantitative T_1 map, calculated based on the bias-free T_1w combination image, sequence parameters and a lookup table. As in the T_1w/PDw approach using MPRAGE, the resulting image ideally is independent of B_1^-, PD, and T_2* effects.

These proposed alternatives minimize scanning time, but also restrict the possible range of sequence parameters, possibly leading to B_1^+-related image inhomogeneity, which needs to be accounted for. Several correction methods have been proposed to counteract the inhomogeneities of the transmit and receive bias fields. These include the use of an optimized adiabatic RF pulse, for example, the time resampled frequency offset compensated inversion (TR-FOCI; Hurley et al., 2010) pulse, and strategically placed dielectric pads to improve inversion efficiency in low B_1^+ regions (Teeuwisse, Brink, & Webb, 2012). In addition, *post-hoc* methods, for example, low-pass filtering, low-order fitting of the images (Ashburner & Friston, 2005) and/or computing the T_1w/PDw ratio image to remove the PD (i.e., M_0), B_1^- and T_2* components (Van de Moortele et al., 2009), are often used to optimize image homogeneity by removing the apparent bias field. However, even though image inhomogeneities are largely accounted for by these MRI acquisition solutions or postprocessing methods, image imperfections and classification biases may still persist. In addition, the image-based bias field removal methods discussed above will not result in more correct T_1 quantification, but only improves low spatial-frequency image homogeneity. Therefore, Weiskopf et al. (2011) combined an unified segmentation-based correction of T_1 maps —acquired using an 3D FLASH with variable excitation flip angles (VFA) —for residual B_1^+ inhomogeneities. Alternatively, an additional B_1^+ map can be acquired to *post-hoc* improve B_1^+ independence, as reviewed by Lutti, Hutton, Finsterbusch, Helms, and Weiskopf (2010) and Pohmann and Scheffler (2013), which is able to cover a broader range of T_1 mapping sequences. For the MP2RAGE sequence, the use of different (low) flip angles for the GRE images (α_1 and α_2) renders the MP2RAGE T_1 map largely, but not entirely, free from B_1^+ effects. Here, correction using the Saturation-prepared with 2 rapid Gradient Echoes (Sa2RAGE) sequence has been used to remove residual B_1^+ effects (Eggenschwiler, Kober, Magill, Gruetter, & Marques, 2012; Marques & Gruetter, 2013).

Initial work has shown that *post-hoc* B_1^+ correction of MP2RAGE maps improves the subcortical GM vs. WM contrast-to-noise ratio (CNR) facilitating automatic segmentation (Marques & Gruetter, 2013). However, the effect of this correction scheme has not yet been extensively characterized across cortical regions. Based on the initial results by Marques et al. (2017) and the B_1^+ correction methodology, the difference in the degree of T_1(w) signal changes depends on the apparent T_1 value and, therefore, vary between WM and GM, even if the voxels are very close to each other. As such, the correction also affect the CNR between cortical GM and WM, and we expect this to propagate toward differences in the cortical surface reconstructions and, therefore, apparent cortical thickness. Thus, the aim of this study is to quantify the changes of cortical thickness, and the underlying changes in

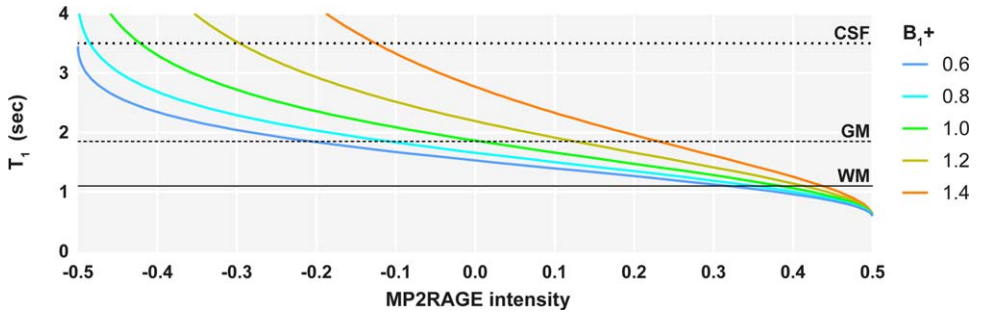

FIGURE 1 MP2RAGE B_1^+ dependency. B_1^+ dependency of the T_1 map for a range of B_1^+ values (colored solid lines). Typical WM, GM, and CSF T_1 values are indicated using the vertical lines [Color figure can be viewed at wileyonlinelibrary.com]

estimated T_1[1], after applying the proposed B_1^+ correction method. To quantify the effect of removing residual B_1^+ bias, the longitudinal analysis stream within the newly released FreeSurfer v6.0 was used (Reuter & Fischl, 2011). This allows high-resolution (<1 mm^3) surface reconstructions of the B_1^+ uncorrected and corrected MP2RAGE data, which are consequently directly comparable due to matching topology and number of vertices, using surface-based analysis approach similar as in Fujimoto et al. (2014). Finally, subsequent regional cortical thickness averages are compared to normative data based on the model presented in Potvin et al. (2017) to evaluate their accuracy. The model provides subject-specific cortical thickness estimates for cortical regions based on the subject's demographics and scanner characteristics.

2 | MATERIALS AND METHODS

2.1 | Subjects and data acquisition

Sixteen healthy volunteers (age = 39 ± 13.8, between 20 and 66 years old, 4 males) were included in this study after providing written informed consent in accordance with the Declaration of Helsinki. The protocol was approved by the ethics review board of the Faculty of Psychology and Neuroscience, Maastricht University, the Netherlands. MRI data were acquired using a whole-body 7T magnet (Siemens Healthineers, Erlangen, Germany) and a 32-channel phased-array head coil (Nova Medical, Wilmington, MA, USA). High resolution (0.7 mm isotropic nominal voxel size) whole-brain quantitative T_1 images were obtained with the MP2RAGE (Marques et al., 2010) sequence, and the Sa2RAGE (Eggenschwiler et al., 2012) sequence was used to map B_1^+ (2 mm isotropic nominal voxel size) across the brain. MP2RAGE data were acquired with TR/TE = 5,000/2.47 ms, TI_1/TI_2 = 900/2,750 ms, $\alpha_1/\alpha_2 = 5°/3°$ and generalized autocalibrating partially parallel acquisitions (GRAPPA) factor = 3 in the phase-encoding (PE) direction (anterior–posterior) with 24 references lines. For the Sa2RAGE, the parameters were: TR/TE = 2,400/0.78 ms, TD_1/TD_2 = 58/1,800 ms, $\alpha_1/\alpha_2 = 4°/11°$, and GRAPPA factor = 2 in PE direction (anterior–posterior) with 24 references lines. See Haast, Ivanov, Formisano, and Uludag (2016) for further details on other scanning parameters. The TR-FOCI inversion pulse (Hurley et al., 2010) and dielectric pads containing a 25% suspension of barium titanate in deuterated water, placed around the head proximal to the temporal lobe areas (Teeuwisse et al., 2012), were used to improve B_1^+ homogeneity across the brain and locally, respectively.

2.2 | Preprocessing pipeline

Several preprocessing steps were performed to improve subsequent automatic segmentation. First, the data were skull-stripped by using the different MP2RAGE output volumes (UNI, T_1 map and INV2; see Marques et al., 2010). The INV2 (i.e., PDw) image was used to obtain a brain mask, as it provides the best intra- and extracranial tissue contrast, especially after removal of any RF bias field using ANTs' (Advanced Normalization Tools) N4BiasFieldRemoval tool (Tustison et al., 2010). Remaining non-brain tissue was removed using probability maps of the dura mater and arteries. These initial steps were performed using MIPAV 7.1.1 (Center for Information Technology, NIH, Bethesda, MD, USA), JIST 3.0 (Johns Hopkins University, Baltimore, MD, USA) and CBS High-Res Brain Processing tools 3.0.9 (Max Planck Institute for Human Cognitive and Brain Sciences, Leipzig, Germany). Both the MP2RAGE UNI and T_1 images were *post-hoc*-corrected for variations in B_1^+ using the same method, as described in Marques and Gruetter (2013)[2]. Briefly, the "original" MP2RAGE UNI volume and Sa2RAGE B_1^+ map were used to generate the "corrected" UNI image and T_1 map. Given the higher independence of B_1^+ estimation on the T_1 values, the B_1^+ map was first optimized for the varying T_1 across the brain using 2D interpolation and the Sa2RAGE lookup table. This newly generated B_1^+ map was consecutively used to generate a T_1 map by taking into account the varying B_1^+ across the brain using 2D interpolation and the MP2RAGE lookup table. This process was repeated three times and, as in the original paper, variations in both B_1^+ and T_1 were found to be under 10^{-3} for the last iteration. The B_1^+ dependency plot of the T_1 map for the current sequence parameters is displayed in Figure 1.

Noteworthy, by computing the GRE_{TI1} and GRE_{TI2} ratio (i.e., T_1w) image, high background (salt and pepper) noise outside of the brain is

[1]Note that T_1 ideally is an intrinsic and objective property of the tissue and, thus, is not affected by B_1^+ correction. Therefore, when referring to changes in calculated T_1 values throughout the manuscript, it should read "changes in apparent/measured T_1" and not "changes in intrinsic T_1."

[2]The code used to perform the B_1^+ correction is publicly available at https://github.com/JosePMarques/MP2RAGE-related-scripts.

introduced, in addition to increased noise in the meninges (O'Brien, Krueger, Lazeyras, Gruetter, & Roche, 2013). These can be masked out, but differences in the noise- and T_1-dependent CNR, induced after the B_1^+ correction step, can also affect the performance of the skull-stripping algorithms. In particular, in thin cortical regions (e.g., near the occipital cortex), the GM is not easily separable from other structures, such as the dura mater and cerebral sinuses, because of the comparable image intensity. In order to eliminate any additional methodological bias related to this and to tie the differences purely to changes in T_1 and CNR, the same subject-specific binary brain mask was used for both datasets. Gradient nonlinearity correction without jacobian intensity correction (to preserve the quantitative T_1 values) was applied on the brain extracted B_1^+ corrected MP2RAGE UNI and other (including the original) volumes using the gradient coefficients file provided by the scanner manufacturer and the Human Connectome (HCP) high-res analysis "gradunwarp" tool (https://github.com/Washington-University/gradunwarp). Finally, the skull-stripped and gradient distortion unwarped MP2RAGE UNI volumes were aligned using affine transformation to the MNI space (0.7 mm) template prior to cortical surface reconstruction.

2.3 | Surface reconstruction pipeline

High-resolution cortical reconstruction was performed with the longitudinal processing stream implemented in the FreeSurfer (v6.0, http://surfer.nmr.mgh.harvard.edu/) image analysis suite (Dale et al., 1999; Reuter, Schmansky, Rosas, & Fischl, 2012). This was necessary to enable direct (i.e., vertex-by-vertex) comparison between the surface reconstructions and cortical thickness surface metric based on either the original or B_1^+ corrected MP2RAGE UNI images. First, a template volume was computed using both images to obtain initial white matter (WM-GM boundary) and pial (GM-CSF) surfaces (Reuter & Fischl, 2011). These surfaces were then aligned with the original and corrected volumes, whose intensity values were subsequently used to deform surfaces following the same procedure as in the standard FreeSurfer processing stream. Please note that computation of the template surfaces is crucial to obtain a "bias-free" starting point for generating surfaces optimized for either the original or the corrected volumes. This resulted in two different datasets, but with matching mesh topology and the same number of vertices. No manual corrections were performed to avoid bias toward one of the datasets.

2.4 | Postprocessing pipeline

For each subject, the WM and pial surfaces (derived from the corrected MP2RAGE dataset) and associated cortical thickness map were used to project the (original and corrected) T_1 and B_1^+ maps onto the surface. This was done using FreeSurfer's *mri_vol2surf* function and by averaging between 20 and 80% of the cortical thickness (with steps of 0.05%) to reduce partial voluming with WM and CSF. Subsequently, T_1 and cortical thickness difference maps were calculated by subtracting the values based on the original maps from that of the corrected maps. In addition, for each vertex and (white and pial) surface, the change in the vertex's location (in mm, along the vertex's normal) for the corrected (vs original) volume was computed and projected onto the surface (Fujimoto et al., 2014). All surface maps were coregistered to the "fsaverage" subject using sphere-based alignment (Fischl, Sereno, Tootell, & Dale, 1999) for further (statistical) analyses. Final surface maps were visualized using the Connectome Workbench v1.2.3 viewer (Washington University School of Medicine, Saint Louis, MO, USA) after conversion of the inflated surfaces and overlays to a compatible format. Noncortical vertices in between hemispheres were masked out using FreeSurfer's parcellation scheme and excluded from the comparisons. In addition, region-wise comparisons of average T_1 (including inter-regional coefficient of variation) and cortical thickness were performed following the parcellation provided by FreeSurfer (i.e., "Desikan-Killiany Atlas"; Desikan et al., 2006). Finally, to test the accuracy of the cortical thickness measures, normative cortical thickness data were calculated using the model presented in Potvin et al. (2017). For each subject, estimates of their expected regional cortical thickness based on age, gender and estimated total intracranial volume and the scanner characteristics were obtained. In the current study, scanner manufacturer was set to "Siemens" and magnetic field strength to "3T," the highest possible. This resulted in a set of normative cortical thickness data, which can account for different ages and gender. MATLAB (R2015B, The MathWorks, Natick, Massachusetts, USA) was used to compute the Euclidean distance, d, between the two vectors (i.e., $\vec{u}$, normative data and $\vec{v}$, cortical thickness based on original or corrected data) across all subjects, n, for each region:

$$\boldsymbol{d}(\vec{\boldsymbol{u}},\vec{\boldsymbol{v}}) = \| \vec{\boldsymbol{u}} - \vec{\boldsymbol{v}} \| = \sqrt{(\boldsymbol{u}_1 - \boldsymbol{v}_1)^2 + (\boldsymbol{u}_2 - \boldsymbol{v}_2)^2 \ldots (\boldsymbol{v}_n - \boldsymbol{v}_n)^2} \quad (1)$$

For each region, the difference in Euclidean distance (i.e., $d_{\text{diff}} = d_{\text{original}} - d_{\text{corrected}}$) was mapped onto an inflated surface to indicate whether the average cortical thickness became more comparable (i.e., $d_{\text{diff}} > 0$ in red/yellow) or less comparable (i.e., $d_{\text{diff}} < 0$ in blue/green) to the normative data after the B_1^+ correction.

2.5 | Statistical analyses

Whole-brain vertex-wise analyses using FreeSurfer's QDEC tool were performed to detect vertices characterized by a significant (false discovery rate (FDR)-corrected) change in T_1 and/or cortical thickness after B_1^+ correction. In addition, pairwise t tests and MATLAB were used to test for statistical differences in average T_1 or cortical thickness across the entire GM or per region, between the original and corrected data. Finally, correlation coefficients between original or corrected and normative cortical thickness data were calculated.

3 | RESULTS

Figure 2a shows the cross-sectional (axial) images from the original (first column) and corrected (second) MP2RAGE T_1 maps, corresponding corrected-original T_1 difference (third) and B_1^+ map (last) from a single-subject, for illustrative purposes. Most pronounced T_1 changes (mostly decrease, in green) were mainly observed along the cortex and clearly reflected the differences of B_1^+ across the brain based on the

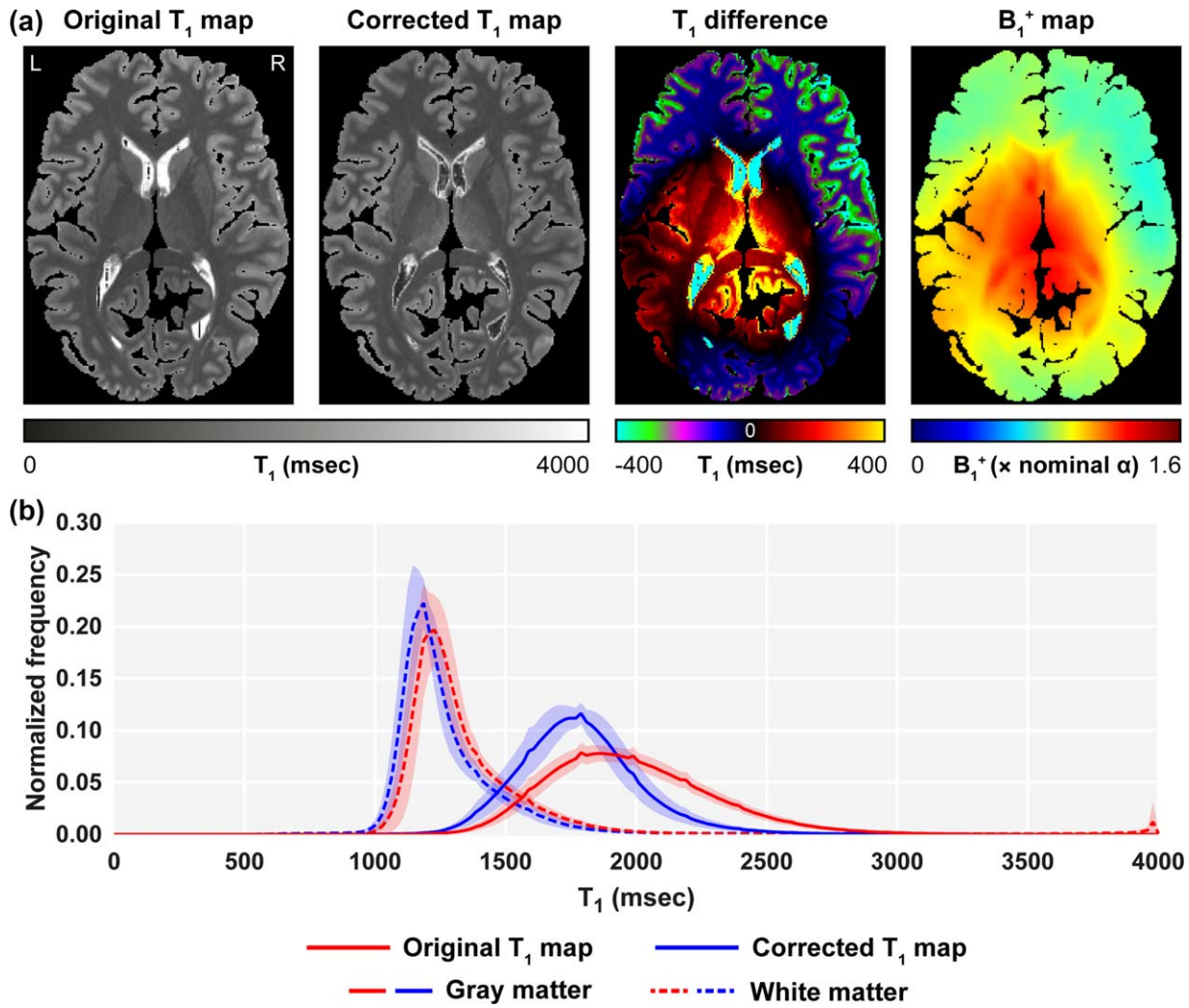

FIGURE 2 MP2RAGE and Sa2RAGE volume data. Example original and corrected MP2RAGE T_1 maps (ms), the difference between them (ms), and corresponding B_1^+ map (× nominal value) are shown (left to right, b). Normalized (for number of voxels) grey (solid lines) and white matter (dashed) T_1 distributions (averaged across subjects, ±*SD*) are shown for both the original (red lines) and corrected (blue) T_1 maps (b). Here, the same tissue masks (based on the corrected data) were used to compute the T_1 histograms for the original and corrected data [Color figure can be viewed at wileyonlinelibrary.com]

correspondence with the B_1^+ map. This was confirmed by the clear change of the GM (solid lines) and WM (dashed) T_1 distributions (averaged across subjects after normalization for the number of voxels) obtained from the B_1^+-corrected (blue) versus that of the original (red) T_1 maps (Figure 2b). It is apparent that the variance and the mean of the T_1 values reduce for GM and less for WM after taking B_1^+ into account. As such, the area of the overlap between the GM and WM histograms for the entire brain increased after the B_1^+ correction (0.534 ± 0.07 vs 0.592 ± 0.06, paired t test, $t_{15} = 10.59$, $p < .0001$). However, when only the temporal lobe is considered (histograms not shown), this significantly decreased (0.435 ± 0.08 vs 0.372 ± 0.09, paired t test, $t_{15} = 8.81$, $p < .0001$), indicating improved separability of GM and WM. No significant difference was observed for the cingulate cortex (0.265 ± 0.07 vs 0.262 ± 0.08).

To better appreciate the distribution of the observed changes, surface representations of the original and corrected T_1 maps are shown in Figure 3a,b for the left hemisphere. As very similar observations are made for the right hemisphere, the respective data are shown in Supporting Information, Figure 1. Note that the same scaling for both original (mean surface-based GM $T_1 = 1{,}944.6 \pm 223.1$ ms) and corrected T_1 (1,794.3 ± 124.8 ms, paired t test, $t_{15} = 7.966$, $p < .0001$) maps was applied to be able to directly compare T_1 values based on the color scheme. Here, a gradient toward higher values (e.g., from green to yellow/red) in more inferior parts of the brain was observed in the original data, which mirrors the observed variation of B_1^+ across the cortex (Figure 3e). This gradient was not visible in the corrected T_1 maps. After the B_1^+ correction, T_1 most significantly (vertex-wise comparison, FDR-corrected $p < .05$) decreased in the inferior affected areas (e.g., inferior temporal and frontal lobes), but increased (although to a smaller extent) in the posterior cingulate cortices and left parietal lobe (the latter for left hemisphere only) compared to the original T_1 maps (Figure 3c,d). On average, cortical T_1 was changed −150.3 (± 73.1) ms after the correction.

Region-wise T_1 averages (across subjects ± *SD*) are shown in Figure 4. Regions (*x*-axis) were sorted based on the original T_1 (red lines)

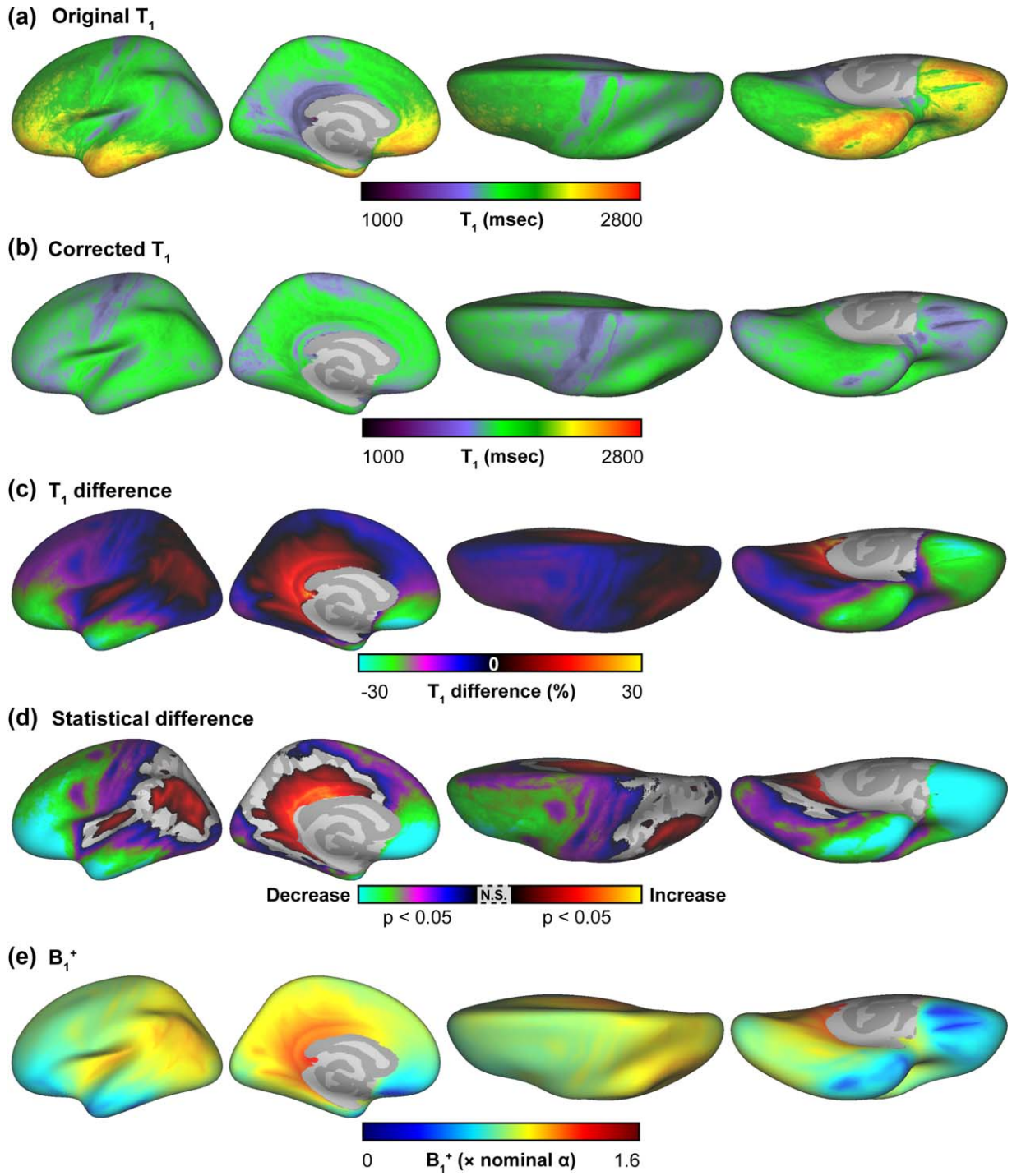

FIGURE 3 Average cortical T_1 surface maps. Original (a) and corrected (b) T_1 (ms), T_1 difference (%, c), statistical difference (d), and B_1^+ (× nominal value, e) were mapped onto an inflated left hemisphere surface and averaged across all subjects. Only vertices with a significant (FDR-corrected $p < .05$) decrease (blue/green) or increase (red/yellow) of T_1 are highlighted in d and grey vertices are nonsignificant (NS) [Color figure can be viewed at wileyonlinelibrary.com]

values (*y*-axis) on the left hemisphere (solid). Vertical lines to the right of the graph indicate the observed range of T_1 values across regions. On average, the original regional T_1 values are within a 904.3 ms range (from 1,521.6 ms to 2,425.9 ms), but this was significantly reduced to 430.2 ms (1,597.4 to 2,027.6 ms, paired *t* test, $t_{15} = 13.69$, $p < .0001$) for the corrected data. This resulted in an inter-regional COV of 0.107 (±0.016) versus 0.040 (±0.005), respectively. In particular, regions with high T_1 values were affected by the B_1^+ correction. Largest region-wise differences in T_1 between the original and corrected data were observed for the temporal and frontal poles and the medial orbitofrontal sulci and inferior temporal gyri.

To illustrate the effect of the B_1^+ correction on the cortical segmentation, both sets (original, in red, and corrected, in blue) of white matter (left column) and pial (right) surfaces were overlaid onto a

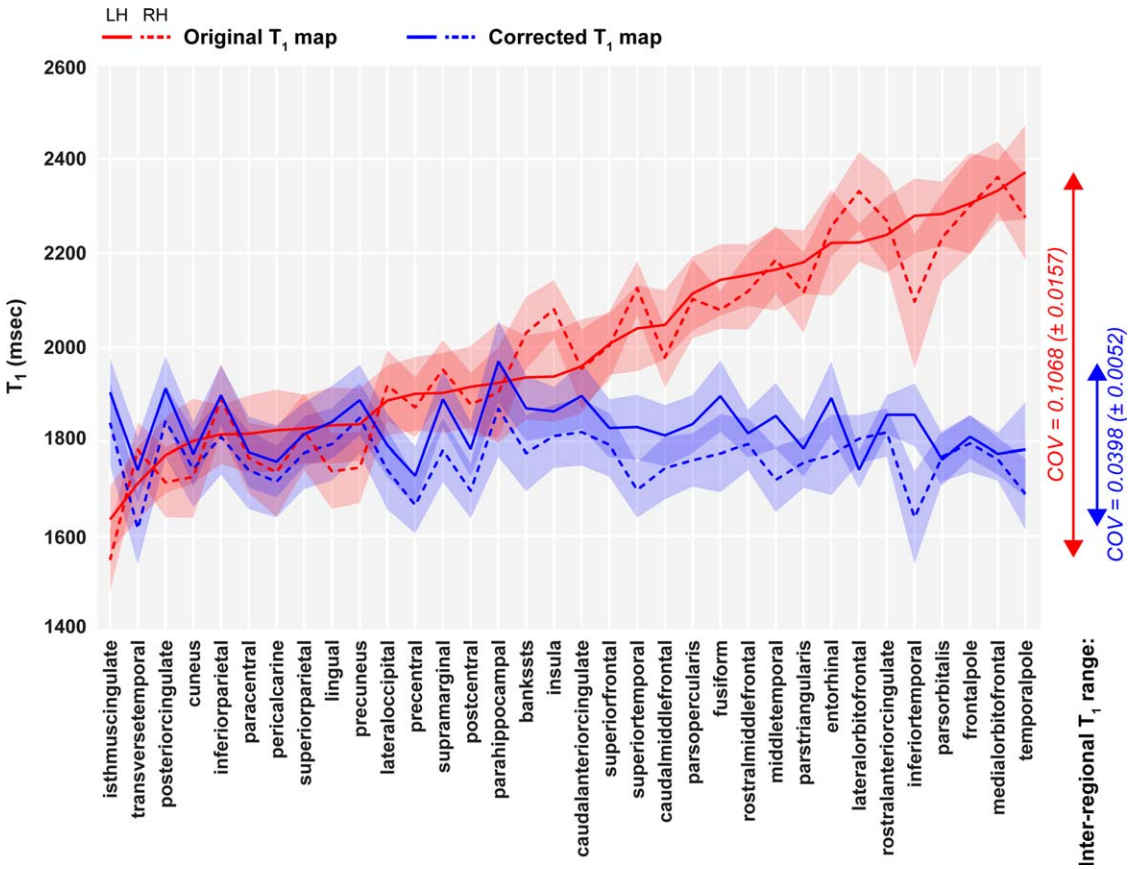

FIGURE 4 Regional T_1 averages before and after B_1^+ correction. Original (red lines) and corrected (blue) across subjects T_1 averages (*y*-axis, ms $\pm SD$) are plotted across all regions (*x*-axis) for both the left (solid lines) and right (dashed) hemispheres. Regions are sorted based on the original T_1 map. Vertical lines to the right of the graph indicate the region-wide range of T_1 values and corresponding inter-regional coefficient of variation [Color figure can be viewed at wileyonlinelibrary.com]

coronal slice (of the temporal lobe at the location of the dashed line) of the B_1^+-corrected MP2RAGE T_1 map (see Figure 5a for a single-subject example, and Supporting Information, Figure 2 for additional examples from multiple subjects). The distance (in mm, e.g., indicated by white double arrow) along the vertex's normal between original and corrected surfaces was then mapped onto the surface for the left hemisphere (see Figure 5b and Supporting Information, Figure 3 for right hemisphere), so that negative values indicated inward movement (i.e., toward the centre of the brain) while positive values indicated outward movement of the surface for the corrected data. While both the (left and right) WM and pial surfaces followed the same pattern, a stronger effect was observed for the pial surface, for which, especially in the inferior frontal and temporal lobes, the surface expanded (shown in red/yellow). On the other hand, both WM and pial surfaces were placed more inward after correction (shown in blue) in the vicinity of the posterior cingulate cortices. On average, the WM and pial surfaces were moved by −0.104 (± 0.054, see black histograms in Figure 5c) and 0.255 (± 0.092, green) mm, and the corresponding distributions showed a slight bias toward negative and positive values, respectively.

Figure 6a,b shows the resulting cortical thickness maps computed from the surfaces derived from the original or corrected data, respectively. Mean cortical thickness (across the entire ribbon) for the original data was significantly lower (2.117 ± 0.053 mm) than the cortical thickness based on the corrected data (2.282 ± 0.06 mm, paired *t* test, $t_{15} = 11.69$, $p < .0001$). Most significant differences in cortical thickness (Figure 6c) were observed in the inferior frontal and temporal lobes (vertex-wise comparison, FDR-corrected $p < .05$, see Figure 6d). Again, comparable differences were observed across hemispheres, except the decreased cortical thickness in the parietal lobe did not reach the significance level for the right hemisphere (Supporting Information, Figure 4).

In addition, left and right hemisphere average (across subjects) cortical region T_1 and thickness changes (in %) were inversely correlated (Pearson correlation, $r_{33} = -0.870$, $p < .001$ and $r_{33} = -0.839$, $p < .001$, respectively). That is, a T_1 decrease after B_1^+ correction led to an increase in measured cortical thickness (Figure 7 and Supporting Information, Figure 5).

Finally, to benchmark the accuracy of the cortical thickness measurements, regional cortical thickness data were compared to the normative data calculated based on the demographics of the study population (see green dots in Supporting Information, Figure 6a). Please note that normative data could not be computed for the banks of superior temporal sulcus (i.e., "bankssts"), frontal, and temporal poles. In general, more close agreement with the normative values (green filled circles) was reached for the corrected data (blue bars) compared to the

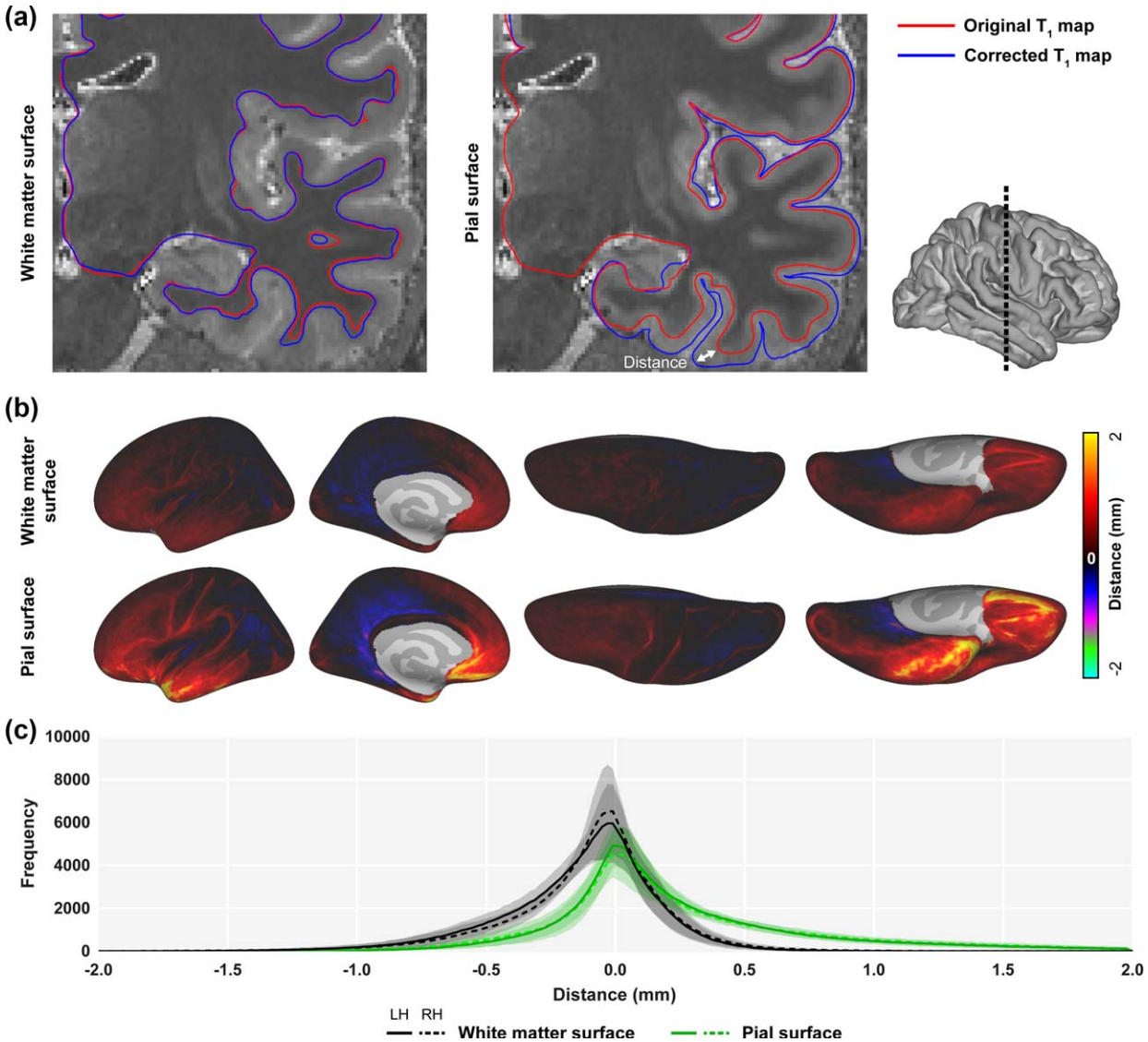

FIGURE 5 White matter and pial surface reconstructions. Example white matter (left) and pial (right) surface reconstructions based on the original (red lines) and corrected (blue) T_1 maps are shown (a). The spatial difference (mm) between both surfaces (white matter: top and pial: bottom), based on the original and corrected data, are mapped onto an inflated left hemisphere surface (b). Average distributions (across subjects $\pm SD$) of these differences are plotted for both white matter (black) and pial (green) surfaces, and left (solid lines) and right (dashed) hemispheres [Color figure can be viewed at wileyonlinelibrary.com]

original data (red bars), especially in the regions where the largest cortical thickness changes were observed (from bottom and up). As such, the correlation between the measured and normative cortical thickness values increased after the B_1^+ correction (Supporting Information, Figure 6b). For each region, the Euclidean distance (across all subjects) between each dataset and the normative dataset was calculated to quantify comparability (Figure 8a). The Euclidean distance was significantly lower for the corrected data compared to the original data for both the left (1.049 ± 0.545 vs 1.761 ± 1.073, paired t test, $t_{30} = 4.126$, $p < .001$) and right (1.019 ± 0.566 vs 1.750 ± 1.100, paired t test, $t_{30} = 4.177$, $p < .001$) hemispheres. The regional quantitative differences were then mapped onto the surface (Figure 8b) to compare with the changes in T_1 and B_1^+ (Figure 3b,e). Here, red/yellow indicates higher comparability while blue/green indicates lower comparability with the normative data. Strongest changes in comparability were observed for regions characterized by pronounced T_1 changes and deviations of B_1^+. Here, the comparability increased for the temporal lobes, but decreased for the anterior cingulate cortex.

4 | DISCUSSION

Despite tremendous improvements, UHF data still suffers from image imperfections related—among other sources—to B_1 inhomogeneities leading to various errors in MRI-based cortical thickness measurements and/or relaxometry (Collins, Li, & Smith, 1998; Marques & Norris, 2017; Padormo, Beqiri, Hajnal, & Malik, 2016; Ugurbil, 2017; Vaughan et al., 2001). In particular, quantitative T_1 mapping approaches ideally allow acquisition of unbiased anatomical data with any influence of scanner imperfections removed, in contrast to conventional T_1w

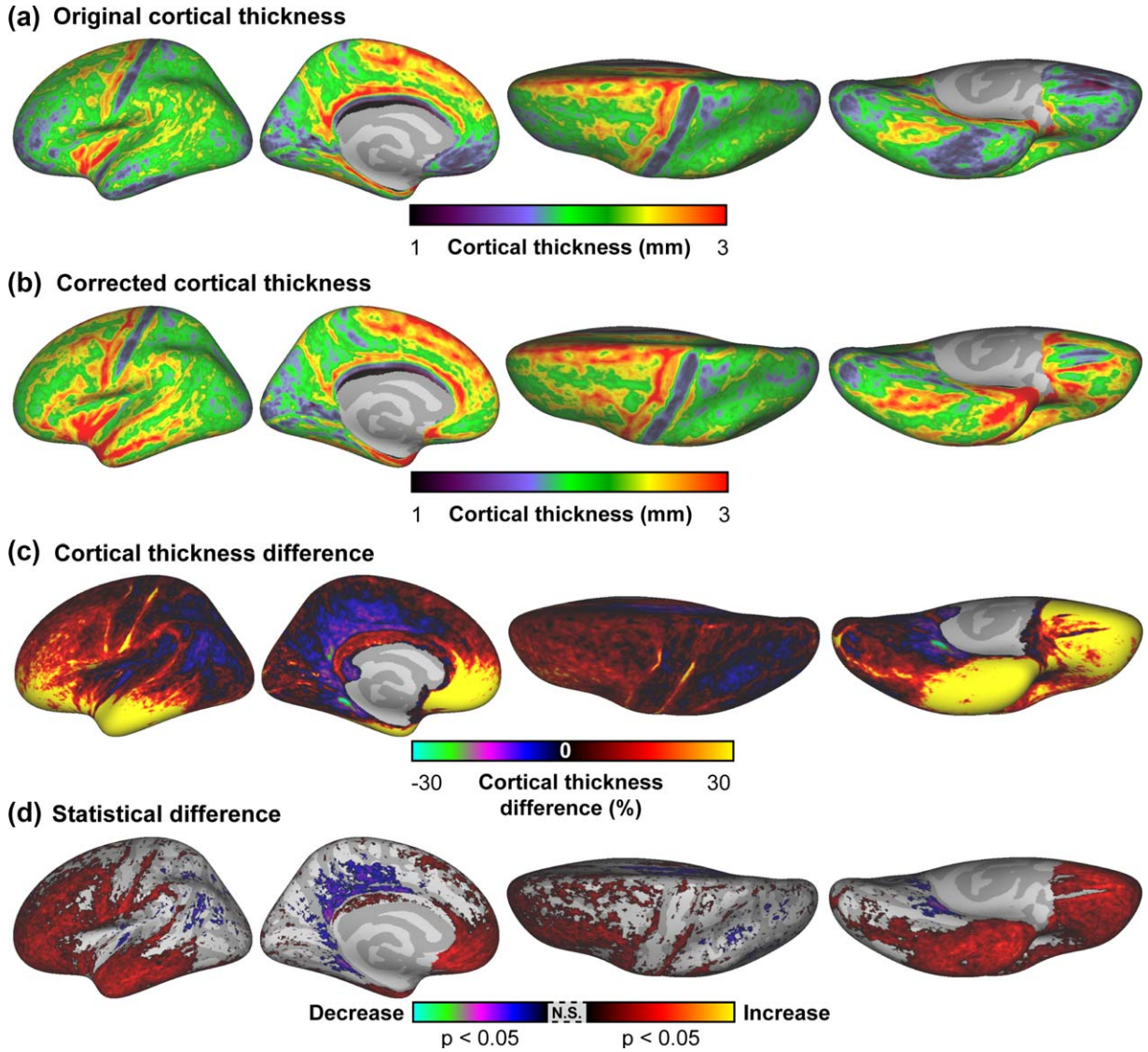

FIGURE 6 Average cortical thickness surface maps. Original (a) and corrected (b) cortical thickness (mm), cortical thickness difference (%, c), and statistical difference (d) were mapped onto an inflated left hemisphere surface and averaged across all subjects. Only vertices with a significant (FDR-corrected $p < .05$) decrease (blue/green) or increase (red/yellow) of cortical thickness are highlighted in (d) and grey vertices are nonsignificant (NS) [Color figure can be viewed at wileyonlinelibrary.com]

images. However, residual B_1^+-related imperfections may still persist for many standard quantitative acquisition schemes.

In this study, we investigated the effect of residual B_1^+ inhomogeneities on T_1 and cortical thickness estimates based on T_1(w) MP2RAGE data. Recently, the MP2RAGE sequence gained popularity at UHF, due to its easy implementation and efficiency to map T_1 at a submillimeter scale without significantly sacrificing SNR (and CNR). The MP2RAGE sequence allows the acquisition of a quantitative T_1 map and T_1w image within a reasonable (i.e., <10 min) time frame (Marques et al., 2010). Whereas the T_1 map can be directly used to quantify microstructural (e.g., myelin)-related changes of the brain (Stuber et al., 2014), the T_1w image can be readily processed by publicly available software, such as the widely used FreeSurfer, to obtain cortical thickness maps (Fischl & Dale, 2000). However, it has been noted that the quantitative T_1 values using the MP2RAGE sequence, similar to other quantitative T_1 approaches, are affected by B_1^- and B_1^+ imperfections. In order to reduce the sensitivity to image inhomogeneities, particularly prominent at UHF, we utilized an adiabatic TR-FOCI inversion pulse together with dielectric pads proximal to the temporal lobes (O'Brien et al., 2014). Nevertheless, the persisting spatially varying B_1^+ field may still lead to an erroneous estimate of T_1 due to deviation of the excitation flip angle from its nominal value, leading to decreased intrasubject reproducibility, and increased across subjects and studies variation of GM and WM T_1 estimates. In addition to errors in T_1 values in general, the GM-WM contrast may be reduced, resulting in erroneous estimation of cortical thickness.

4.1 | B_1^+ dependency of cortical T_1 estimates

MP2RAGE settings are chosen accordingly to specific study aims: T_1 mapping vs. morphometry or a tradeoff between them. For example, to

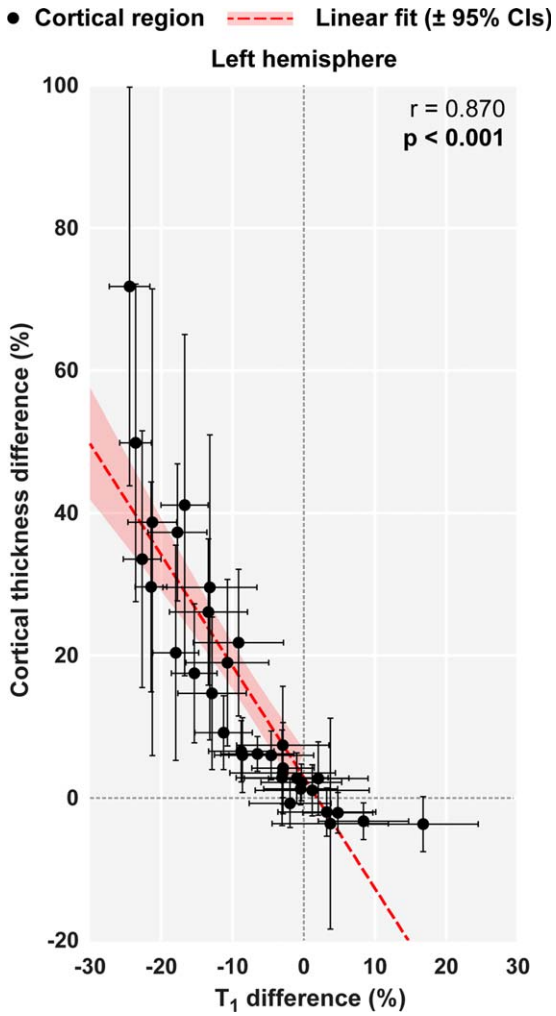

FIGURE 7 Regional T_1 and cortical thickness changes. Across subjects average T_1 (*x*-axis) and cortical thickness (*y*-axis) changes (%, $\pm SD$) are plotted for each region (black dots) for the left hemisphere. Dashed red lines represent the best fit ± 95% CIs. Boldface *p* values indicate a significant correlation [Color figure can be viewed at wileyonlinelibrary.com]

remedy T_1 errors, Marques et al. (2010) provided a set of sequence parameters that limits the B_1^+-dependence of the MP2RAGE sequence, while simultaneously attaining sufficient CNR per unit time for segmentation. However, residual B_1^+ dependency may still persist even for optimized MP2RAGE sequence parameters, as it assumes a homogeneous B_1^+ during T_1 quantification. Note that by comparing the current B_1^+ sensitivity plot with that from the original MP2RAGE papers, the B_1^+ sensitivity of the protocol chosen here is significantly increased (Marques & Gruetter, 2013; Marques et al., 2010). Part of this is likely due to the increased number of excitations per TR because of the higher resolution used in this study (1.0 mm vs 0.7 mm isotropic nominal voxel size). Consecutively, using an iterative *post-hoc* correction method and the Sa2RAGE sequence, these residual inhomogeneities can be reduced by taking into account the spatially varying B_1^+ across the brain (Eggenschwiler et al., 2012; Marques & Gruetter, 2013). While this approach resulted in enhanced visualization of thalamic nuclei and brainstem structures, the effect on the cortical T_1 values and on thickness remained unexplored.

It has been recently shown that the GM and WM T_1 estimates using MP2RAGE becomes more comparable with IR data after the B_1^+ correction (Kashyap, Ivanov, Havlicek, Poser, & Uludag, 2017). That is, this study provided strong evidence that B_1^+ correction is mandatory for MP2RAGE data to achieve accurate T_1 values. At 7 T, using the standard NOVA Medical head coil, the transmit field inhomogeneities can be a result of the human's head eccentricity, but also due to the rapid drop off of the coil's transmit field's z-coverage (O'Brien et al., 2014). The insufficient B_1^+ in the inferior brain regions reduces the inversion efficiency and impairs image quality, apparent by the reduced MP2RAGE intensity and subsequent significant overestimation of T_1, too strong to counteract using the TR-FOCI inversion pulse and dielectric pads. On the other hand, underestimation of T_1 (i.e., high T_1w signal) in regions close to the posterior cingulate cortex are potentially the result of the "central brightening" phenomenon due to constructive interference of traveling B_1^+ waves (Collins et al., 2005). Please note that the observed left–right asymmetry of the B_1^+ field (observed in all subjects) is the result of the coil's design to improve the general homogeneity and reduce the sensitivity to head size and position within the coil (Ledden, Gelderen, & Duyn, 2005). This led to the observed differences in the extent of the T_1 correction between hemispheres, in particular for the parietal lobe. In this study, we found that cortical T_1 was significantly over- (>30%) or underestimated (up to 15%), due to the strongly varying B_1^+, in the inferior temporal and frontal lobes (i.e., low B_1^+) or posterior cingulate cortex (i.e., high B_1^+), respectively.

Overall, the B_1^+ correction led to an improved inter-regional (but also intersubject, data not shown) COV. That is, the variation of T_1 values across the cortex is remarkably low after B_1^+ correction. For a comparison of the intersubject and scan–rescan COV with that of other (quantitative) contrasts (e.g., T_2*), we refer the reader to Haast et al. (2016). The reduction of the superior-to-inferior gradient of low-to-high T_1—that led to the initially high COV across regions—resulted in a cortical T_1 distribution that is more comparable with previous studies at lower field strengths and are less affected by B_1^+ effects, revealing the typical myelin-related cortical pattern (Glasser & Van Essen, 2011; Lutti, Dick, Sereno, & Weiskopf, 2014). However, even after taking the B_1^+ spatial profile into account, residual T_1 errors persisted across the whole cortex. In the specific case, for which the adiabatic condition was not met, such as in the most inferior part of the temporal lobe (i.e., that suffered from too low B_1^+), T_1 remained artificially low. Additionally, local susceptibility gradients near these regions due to, for example, the spatial proximity to air–tissue interfaces, may hamper the inversion efficiency via B_0-related problems.

4.2 | B_1^+ and T_1 dependency of cortical thickness estimates

Errors in the spatially varying T_1(w) image contrast due to B_1^+ inhomogeneity hamper subsequent anatomical analyses, necessary to obtain biomarkers of cortical atrophy due to aging or disease. In this context, cortical thickness is a popular surface-based metric that is typically computed based on the minimal distance (in mm) between the WM/GM and GM/CSF boundary surfaces (Fischl & Dale, 2000; Jones,

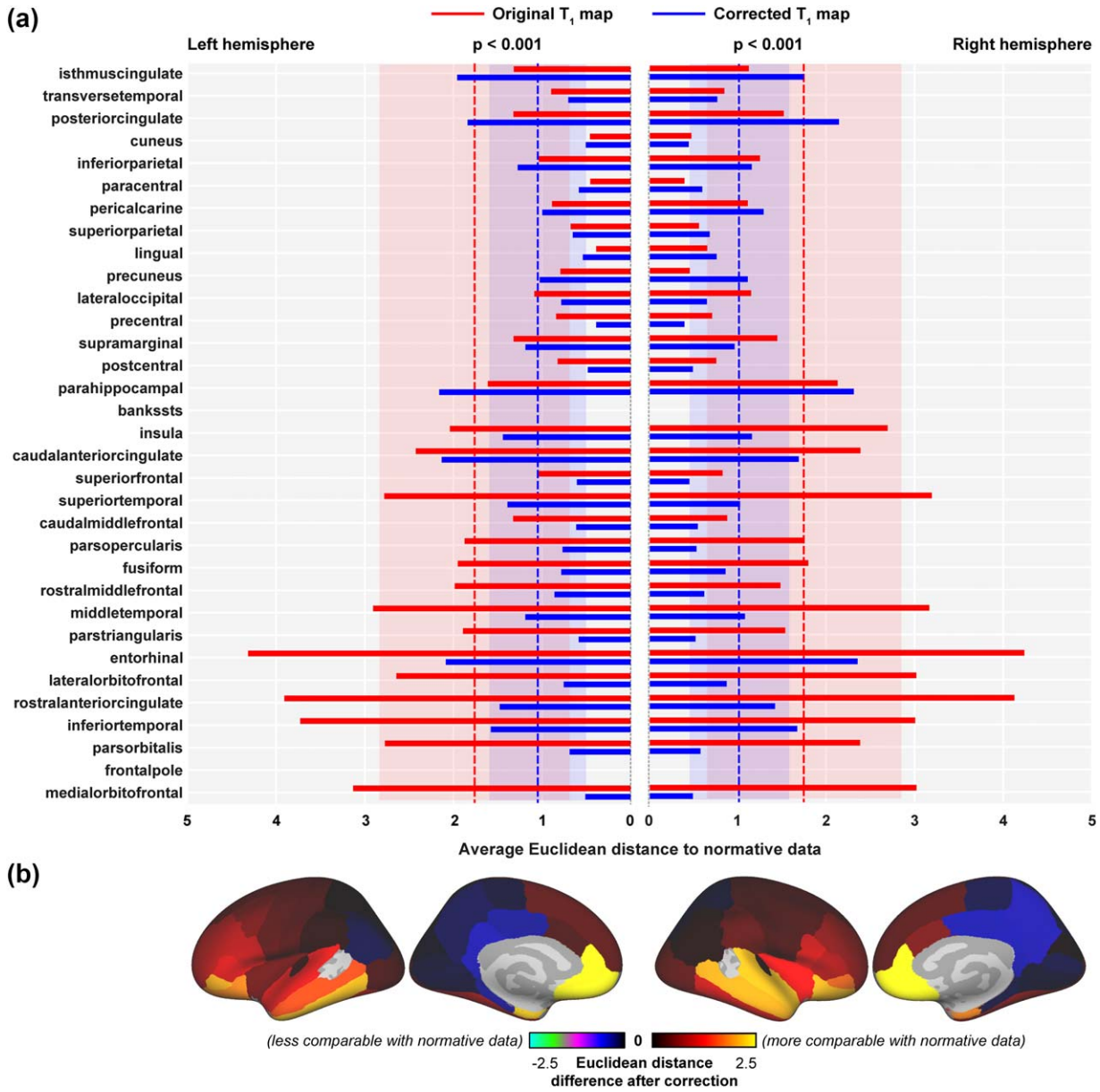

FIGURE 8 Comparison between regional cortical thickness averages with normative data. Euclidean distances between original (red bars) and corrected (blue) cortical thickness averages (*x*-axis) and normative data are plotted across all regions (*y*-axis) for both the left (left column) and right (right) hemispheres. Vertical dashed lines indicate the average Euclidean distance across all regions for original (red) and corrected (blue) T_1 maps, while *p* values on top of the graph indicate the significance level after pairwise comparison across regions. Regions are sorted based on the original T_1 map (Figure 3) [Color figure can be viewed at wileyonlinelibrary.com]

Buchbinder, & Aharon, 2000). Cortical thickness measures depend primarily on the fidelity of the underlying data to accurately place the boundary surfaces based on strong intensity gradients between tissue types. However, due to the dominant influence of myelin density on the GM-WM contrast in T_1 contrast-based images, estimation of cortical thickness based on MRI data has often been criticized, especially when its used to study brain development, aging, or disease (Zilles & Amunts, 2015). For example, the myelin-related cortical variation of T_1, myelinated thickness ratio, but also the metric used to compute cortical thickness, introduce an unpredictable inter-areal variation of cortical thickness values, not consistent with that obtained using histological data (Hutton, De Vita, Ashburner, Deichmann, & Turner, 2008; Lerch & Evans, 2005; Rowley et al., 2015; Zilles & Amunts, 2015). As such, spatial variations in T_1 quantification accuracy and image CNR due to B_1^+ inhomogeneities, can affect the accuracy of determining cortical thickness. To quantify this bias, a comparable analysis approach, as utilized in the study by Fujimoto et al. (2014) at 3T and 7T employing the Longitudinal analysis stream within FreeSurfer v6.0, was used. We observed a significant (i.e., >70%) increase in apparent cortical thickness in the inferior temporal and frontal lobes, while it decreased (i.e., up to 5%) near the posterior cingulate cortex after taking into account the B_1^+ profile. These differences originate predominantly from expansion of the pial surface, while the WM surface remained relatively stable, although on occasion it was placed slightly inward. The observed changes in

surface reconstructions imply improvement of spatial homogeneity and CNR of the GM/CSF. This is in close agreement with the work by Fujimoto et al. (2014). In it, the WM and pial surfaces based on B_1^+-uncorrected MP2RAGE data were positioned outside and inside of the reference (MEMPRAGE) surfaces, respectively, similar to our current observations. However, in contrast to this study, Fujimoto et al. (2014) did not use the TR-FOCI pulse for the MP2RAGE acquisitions, neither at 3T nor at 7T. While they were not able to pinpoint the exact reason for these differences, a recent study showed that the use of a correct model for PVE near tissue boundaries in MP2RAGE data is crucial, and, therefore, hinted toward direct effects of T_1 errors on the performance of cortical segmentations algorithms (Duché et al., 2017). The proposed PVE model takes into account the natural variation of T_1 across the cortex as discussed before, leading to a better delineation of the tissue boundaries. Indeed, the present data show that the differences in surface reconstructions and cortical thickness are significantly (inversely) correlated with T_1 errors, highlighting the importance of B_1^+ correction. In other words, these results imply that cortical thickness measurements are less robust in regions where B_1^+ is strongly off from its nominal value. The reduced contrast between tissue types led to pronounced differences in cortical thickness after the B_1^+ correction, within regions, but also across subjects.

To assess the improvement due to B_1^+ correction and evaluate and benchmark our findings, we compared cortical thickness values in the current study with those of the cortical thickness model developed by Potvin et al. (2017), based on 2757 cognitively healthy controls aged 18–94 years. The model incorporates age, sex, estimated total intracranial volume, magnetic field strength and scanner vendor information to estimate subject-specific regional cortical thickness averages. Age, but also extrinsic factors, such as field strength and scanner platform, may affect cortical thickness estimates and are, therefore, important to take into account (Govindarajan, Freeman, Cai, Rahbar, & Narayana, 2014; Han et al., 2006; Lusebrink, Wollrab, & Speck, 2013; Potvin et al., 2017). To quantify the accuracy, we computed the Euclidean distance for each region between the normative data and the average cortical thickness derived from either the original or corrected data across all subjects. The B_1^+ correction improved the correspondence with the normative data, especially in the problematic regions, that is, those characterized by the largest T_1 errors. Despite these improvements, our measurements were systematically lower than assumed using the model, except for those where B_1^+ was close to the nominal value. This suggests that B_1^+ inhomogeneity is the main source for the discrepancy with the normative data. However, it is important to remember that the model does not represent the ground truth, as image biases in the model's underlying data could have led to overestimation of cortical thickness and should, therefore, be considered more as a benchmark. The thicker estimates of the cortex using the model could have potentially originated from the T_2^* and PD contrast present in the data used for the model, which, in contrast, are eliminated in the current MP2RAGE data. For example, variations in cortical thickness measurements were observed after removal of the PD component from T_1w images (Lorio et al., 2016). Nevertheless, two other important factors, both related to the spatial resolution of the input data, could have contributed to the slight discrepancy of our results to those of Potvin et al. (2017). First, in contrast to our 7T submillimeter data, the model is based on lower field strength and lower spatial resolution data. Therefore, this model may not be fully applicable to our 7T data, even though the study of Potvin et al. (2017) did not detect field strength dependency of cortical thickness estimates based on 1.5T and 3T data. Also, increased PVE, due to the lower resolution, may have slightly overestimated the cortical thickness obtained using the 1.5T and 3T datasets. In accordance with this, significantly reduced thickness has previously been determined using submillimeter data compared to 1 mm^3 (ME)MPRAGE data at 7 T, providing evidence for this spatial resolution effect (Lusebrink et al., 2013; Zaretskaya, Fischl, Reuter, Renvall, & Polimeni, 2017). Secondly, FreeSurfer v6.0 was used in the current study, which enables analysis of the data at the native resolution (0.7 mm^3), whereas FreeSurfer v5.3, which was used to develop the model, conforms the data (which ranged from 0.3 to 2.3 mm^3 for the data used to develop the model) to 1 mm^3 resolution and by this means, affecting the spatial specificity. For example, CSF could be misclassified as GM in narrow sulci and therefore lead to overestimation of the cortical thickness, such as seen for the normative data. However, similar differences were observed when analyses were repeated using FreeSurfer v5.3 for a subset of the subjects. Based on the arguments above, the observed discrepancy between the measured cortical thickness and the normative data results presumably from several factors. In case B_1^+ matches its nominal value, the MP2RAGE data remains unchanged after the correction. In addition, due to the folding of the GM ribbon, partial volume effects are random and the measured cortical thickness is comparable with the normative data, even if acquired with a slightly different spatial resolution. However, additional (competing) effects of T_2^* and/or PD in model's data may lead to a higher correlation with our data in regions where B_1^+ is not close to its nominal value. Please note that this issue is not the main focus of this article and would require a more systematic investigation.

5 | CONCLUSION

The accuracy of MRI-based measurements of cortical thickness are directly dependent on the T_1(w) image quality. As such, B_1^+-related inhomogeneities in UHF MRI data significantly affect cortical T_1 and thickness estimates. In the specific case of MP2RAGE data, correction for the varying B_1^+ across the cortex predominantly decreased apparent T_1, leading toward increased and more accurate cortical thickness measurements in the lower frontal and temporal lobe regions. Here, the automatic estimation of cortical thickness is mostly improved due to a better delineation of the GM-CSF boundary through more homogenous apparent T_1 and improved CNR. Taken together, correction for MR image imperfections harbors profound implications for clinical neuroscientific studies interested in disease- and/or age-related microstructural and morphological changes and should be taken into account when setting up imaging protocols and analysis pipelines.

ACKNOWLEDGMENTS

This work was supported by Maastricht University, the Netherlands Organization for Scientific Research (NWO; VIDI grant 452-11-002)

and Technology Foundation STW (12724). The authors are indebted to Prof. Dr Andrew Webb (Leiden University Medical Centre, Leiden, Netherlands) and Dr José Marques (Donders Institute for Brain, Cognition and Behaviour, Nijmegen, Netherlands) for providing the dielectric pads and the MATLAB code to perform the *post-hoc* T_1 correction used in this study, respectively.

CONFLICT OF INTEREST

The authors declare no conflict of interest.

ORCID

Roy A.M. Haast http://orcid.org/0000-0001-8543-2467
Dimo Ivanov http://orcid.org/0000-0001-9387-5823

REFERENCES

Ashburner, J. (2009). Computational anatomy with the SPM software. *Magnetic Resonance Imaging*, *27*(8), 1163–1174.

Ashburner, J., & Friston, K. J. (2005). Unified segmentation. *NeuroImage*, *26*(3), 839–851.

Bazin, P. L., Weiss, M., Dinse, J., Schafer, A., Trampel, R., & Turner, R. (2014). A computational framework for ultra-high resolution cortical segmentation at 7Tesla. *NeuroImage*, *93*, 201–209.

Collins, C. M., Li, S., & Smith, M. B. (1998). SAR and B1 field distributions in a heterogeneous human head model within a birdcage coil. Specific energy absorption rate. *Magnetic Resonance in Medicine*, *40*(6), 847–856.

Collins, C. M., Liu, W., Schreiber, W., Yang, Q. X., & Smith, M. B. (2005). Central brightening due to constructive interference with, without, and despite dielectric resonance. *Journal of Magnetic Resonance Imaging*, *21*(2), 192–196.

Dale, A. M., Fischl, B., & Sereno, M. I. (1999). Cortical surface-based analysis. I. Segmentation and surface reconstruction. *NeuroImage*, *9*(2), 179–194.

De Martino, F., Moerel, M., Xu, J., van de Moortele, P. F., Ugurbil, K., Goebel, R., … Formisano, E. (2015). High-resolution mapping of myeloarchitecture in vivo: Localization of auditory areas in the human brain. *Cerebral Cortex*, *25*(10), 3394–3405.

De Martino, F., Yacoub, E., Kemper, V., Moerel, M., Uludag, K., De Weerd, P., … Formisano, E. (2017). The impact of ultra-high field MRI on cognitive and computational neuroimaging. *NeuroImage*.

Deoni, S. C., Rutt, B. K., & Peters, T. M. (2003). Rapid combined T1 and T2 mapping using gradient recalled acquisition in the steady state. *Magnetic Resonance in Medicine*, *49*(3), 515–526.

Desikan, R. S., Segonne, F., Fischl, B., Quinn, B. T., Dickerson, B. C., Blacker, D., … Killiany, R. J. (2006). An automated labeling system for subdividing the human cerebral cortex on MRI scans into gyral based regions of interest. *NeuroImage*, *31*(3), 968–980.

Despotovic, I., Goossens, B., & Philips, W. (2015). MRI segmentation of the human brain: Challenges, methods, and applications. *Computational and Mathematical Methods in Medicine*, *2015*, 450341.

Duché, Q., Saint-Jalmes, H., Acosta, O., Raniga, P., Bourgeat, P., Doré, V., … Salvado, O. (2017). Partial volume model for brain MRI scan using MP2RAGE. *Human Brain Mapping*, *38*(10), 5115–5127.

Eggenschwiler, F., Kober, T., Magill, A. W., Gruetter, R., & Marques, J. P. (2012). SA2RAGE: A new sequence for fast B1+ -mapping. *Magnetic Resonance in Medicine*, *67*(6), 1609–1619.

Fischl, B., & Dale, A. M. (2000). Measuring the thickness of the human cerebral cortex from magnetic resonance images. *Proceedings of the National Academy of Sciences of the United States of America*, *97*(20), 11050–11055.

Fischl, B., Salat, D. H., van der Kouwe, A. J. W., Makris, N., Ségonne, F., Quinn, B. T., & Dale, A. M. (2004). Sequence-independent segmentation of magnetic resonance images. *NeuroImage*, *23*, S69–S84.

Fischl, B., Sereno, M. I., Tootell, R. B., & Dale, A. M. (1999). High-resolution intersubject averaging and a coordinate system for the cortical surface. *Human Brain Mapping*, *8*(4), 272–284.

Fujimoto, K., Polimeni, J. R., van der Kouwe, A. J., Reuter, M., Kober, T., Benner, T., … Wald, L. L. (2014). Quantitative comparison of cortical surface reconstructions from MP2RAGE and multi-echo MPRAGE data at 3 and 7 T. *NeuroImage*, *90*, 60–73.

Glasser, M. F., & Van Essen, D. C. (2011). Mapping human cortical areas in vivo based on myelin content as revealed by T1- and T2-weighted MRI. *Journal of Neuroscience*, *31*(32), 11597–11616.

Govindarajan, K. A., Freeman, L., Cai, C., Rahbar, M. H., & Narayana, P. A. (2014). Effect of intrinsic and extrinsic factors on global and regional cortical thickness. *PLoS One*, *9*(5), e96429.

Gulban, O. F., Schneider, M., Marquardt, I., Haast, R. A. M., & De Martino, F. (2018). A scalable method to improve gray matter segmentation at ultra high field MRI. *bioRxiv*.

Haast, R. A. M., Ivanov, D., Formisano, E., & Uludağ, K. (2016). Reproducibility and reliability of quantitative and weighted T1 and T2* mapping for myelin-based cortical parcellation at 7 Tesla. *Frontiers in Neuroanatomy*, *10*, 112.

Han, X., Jovicich, J., Salat, D., van der Kouwe, A., Quinn, B., Czanner, S., … Fischl, B. (2006). Reliability of MRI-derived measurements of human cerebral cortical thickness: The effects of field strength, scanner upgrade and manufacturer. *NeuroImage*, *32*(1), 180–194.

Helms, G., Dathe, H., & Dechent, P. (2008). Quantitative FLASH MRI at 3T using a rational approximation of the Ernst equation. *Magnetic Resonance in Medicine*, *59*(3), 667–672.

Helms, G., Kallenberg, K., & Dechent, P. (2006). Contrast-driven approach to intracranial segmentation using a combination of T2- and T1-weighted 3D MRI data sets. *Journal of Magnetic Resonance Imaging*, *24*(4), 790–795.

Hurley, A. C., Al-Radaideh, A., Bai, L., Aickelin, U., Coxon, R., Glover, P., & Gowland, P. A. (2010). Tailored RF pulse for magnetization inversion at ultrahigh field. *Magnetic Resonance in Medicine*, *63*, 51–58.

Hutton, C., De Vita, E., Ashburner, J., Deichmann, R., & Turner, R. (2008). Voxel-based cortical thickness measurements in MRI. *NeuroImage*, *40*(4), 1701–1710.

Jones, S. E., Buchbinder, B. R., & Aharon, I. (2000). Three-dimensional mapping of cortical thickness using Laplace's equation. *Human Brain Mapping*, *11*(1), 12–32.

Kashyap, S., Ivanov, D., Havlicek, M., Poser, B. A., & Uludag, K. (2017). Impact of acquisition and analysis strategies on cortical depth-dependent fMRI. *NeuroImage*.

Lambert, C., Lutti, A., Helms, G., Frackowiak, R., & Ashburner, J. (2013). Multiparametric brainstem segmentation using a modified multivariate mixture of Gaussians. *NeuroImage. Clinical*, *2*, 684–694.

Ledden, P., Gelderen, P., & Duyn, J. (2005). Birdcage volume transmit, eight channel receive array system for brain imaging at 7T. *Proceedings of the International Society for Magnetic Resonance in Medicine*, *13*.

Lerch, J. P., & Evans, A. C. (2005). Cortical thickness analysis examined through power analysis and a population simulation. *NeuroImage*, *24*(1), 163–173.

Liu, J. V., Bock, N. A., & Silva, A. C. (2011). Rapid high-resolution three-dimensional mapping of T1 and age-dependent variations in the non-human primate brain using magnetization-prepared rapid gradient-echo (MPRAGE) sequence. *NeuroImage*, *56*(3), 1154–1163.

Lorio, S., Kherif, F., Ruef, A., Melie-Garcia, L., Frackowiak, R., Ashburner, J., … Draganski, B. (2016). Neurobiological origin of spurious brain morphological changes: A quantitative MRI study. *Human Brain Mapping*, *37*(5), 1801–1815.

Lusebrink, F., Wollrab, A., & Speck, O. (2013). Cortical thickness determination of the human brain using high resolution 3T and 7T MRI data. *NeuroImage*, *70*, 122–131.

Lutti, A., Dick, F., Sereno, M. I., & Weiskopf, N. (2014). Using high-resolution quantitative mapping of R1 as an index of cortical myelination. *NeuroImage*, *93*, 176–188.

Lutti, A., Hutton, C., Finsterbusch, J., Helms, G., & Weiskopf, N. (2010). Optimization and validation of methods for mapping of the radiofrequency transmit field at 3T. *Magnetic Resonance in Medicine*, *64*(1), 229–238.

Marques, J. P., & Gruetter, R. (2013). New developments and applications of the MP2RAGE sequence–focusing the contrast and high spatial resolution R1 mapping. *PLoS One*, *8*(7), e69294.

Marques, J. P., Khabipova, D., & Gruetter, R. (2017). Studying cyto and myeloarchitecture of the human cortex at ultra-high field with quantitative imaging: R1, R2(*) and magnetic susceptibility. *NeuroImage*, *147*, 152–163.

Marques, J. P., Kober, T., Krueger, G., van der Zwaag, W., Van de Moortele, P. F., & Gruetter, R. (2010). MP2RAGE, a self bias-field corrected sequence for improved segmentation and T1-mapping at high field. *NeuroImage*, *49*(2), 1271–1281.

Marques, J. P., & Norris, D. G. (2017). How to choose the right MR sequence for your research question at 7T and above? *NeuroImage*.

Mugler, J. P., 3rd., & Brookeman, J. R. (1990). Three-dimensional magnetization-prepared rapid gradient-echo imaging (3D MP RAGE). *Magnetic Resonance in Medicine*, *15*(1), 152–157.

O'Brien, K. R., Magill, A. W., Delacoste, J., Marques, J. P., Kober, T., Fautz, H. P., … Krueger, G. (2014). Dielectric pads and low- B1+ adiabatic pulses: Complementary techniques to optimize structural T1 w whole-brain MP2RAGE scans at 7 tesla. *Journal of Magnetic Resonance Imaging*, *40*, 804–812.

O'Brien, K., Krueger, G., Lazeyras, F., Gruetter, R., & Roche, A. (2013). A simple method to denoise MP2RAGE. *Proceedings of the International Society for Magnetic Resonance in Medicine*, *21*.

Padormo, F., Beqiri, A., Hajnal, J. V., & Malik, S. J. (2016). Parallel transmission for ultrahigh-field imaging. *NMRi N Biomedicine*, *29*(9), 1145–1161.

Pohmann, R., & Scheffler, K. (2013). A theoretical and experimental comparison of different techniques for B(1) mapping at very high fields. *NMRi N Biomedicine*, *26*(3), 265–275.

Pohmann, R., Speck, O., & Scheffler, K. (2016). Signal-to-noise ratio and MR tissue parameters in human brain imaging at 3, 7, and 9.4 tesla using current receive coil arrays. *Magnetic Resonance in Medicine*, *75*(2), 801–809.

Polimeni, J. R., Renvall, V., Zaretskaya, N., & Fischl, B. (2017). Analysis strategies for high-resolution UHF-fMRI data. *NeuroImage*.

Potvin, O., Dieumegarde, L., & Duchesne, S. Alzheimer's Disease Neuroimaging, I. (2017). Normative morphometric data for cerebral cortical areas over the lifetime of the adult human brain. *NeuroImage*, *156*, 315–339.

Reuter, M., & Fischl, B. (2011). Avoiding asymmetry-induced bias in longitudinal image processing. *NeuroImage*, *57*(1), 19–21.

Reuter, M., Schmansky, N. J., Rosas, H. D., & Fischl, B. (2012). Within-subject template estimation for unbiased longitudinal image analysis. *NeuroImage*, *61*(4), 1402–1418.

Rowley, C. D., Bazin, P. L., Tardif, C. L., Sehmbi, M., Hashim, E., Zaharieva, N., … Bock, N. A. (2015). Assessing intracortical myelin in the living human brain using myelinated cortical thickness. *Frontiers in Neuroscience*, *9*, 396.

Smith, S. M., Jenkinson, M., Woolrich, M. W., Beckmann, C. F., Behrens, T. E., Johansen-Berg, H., … Matthews, P. M. (2004). Advances in functional and structural MR image analysis and implementation as FSL. *NeuroImage*, *23*, S208–S219.

Stuber, C., Morawski, M., Schafer, A., Labadie, C., Wahnert, M., Leuze, C., … Turner, R. (2014). Myelin and iron concentration in the human brain: A quantitative study of MRI contrast. *NeuroImage*, *93*, 95–106.

Teeuwisse, W. M., Brink, W. M., & Webb, A. G. (2012). Quantitative assessment of the effects of high-permittivity pads in 7 Tesla MRI of the brain. *Magnetic Resonance in Medicine*, *67*(5), 1285–1293.

Tustison, N. J., Avants, B. B., Cook, P. A., Zheng, Y., Egan, A., Yushkevich, P. A., & Gee, J. C. (2010). N4ITK: Improved N3 bias correction. *IEEE Transactions on Medical Imaging*, *29*(6), 1310–1320.

Ugurbil, K. (2017). Imaging at ultrahigh magnetic fields: History, challenges, and solutions. *NeuroImage*.

Van de Moortele, P. F., Akgun, C., Adriany, G., Moeller, S., Ritter, J., Collins, C. M., … Ugurbil, K. (2005). B(1) destructive interferences and spatial phase patterns at 7 T with a head transceiver array coil. *Magnetic Resonance in Medicine*, *54*(6), 1503–1518.

Van de Moortele, P. F., Auerbach, E. J., Olman, C., Yacoub, E., Ugurbil, K., & Moeller, S. (2009). T1 weighted brain images at 7 Tesla unbiased for Proton Density, T2* contrast and RF coil receive B1 sensitivity with simultaneous vessel visualization. *NeuroImage*, *46*(2), 432–446.

Vaughan, J. T., Garwood, M., Collins, C. M., Liu, W., DelaBarre, L., Adriany, G., … Ugurbil, K. (2001). 7T vs. 4T: RF power, homogeneity, and signal-to-noise comparison in head images. *Magnetic Resonance in Medicine*, *46*(1), 24–30.

Viviani, R., Pracht, E. D., Brenner, D., Beschoner, P., Stingl, J. C., & Stocker, T. (2017). Multimodal MEMPRAGE, FLAIR, and [formula: See text] segmentation to resolve dura and vessels from cortical gray matter. *Frontiers in Neuroscience*, *11*, 258.

Weiskopf, N., Lutti, A., Helms, G., Novak, M., Ashburner, J., & Hutton, C. (2011). Unified segmentation based correction of R1 brain maps for RF transmit field inhomogeneities (UNICORT). *NeuroImage*, *54*(3), 2116–2124.

Zaretskaya, N., Fischl, B., Reuter, M., Renvall, V., & Polimeni, J. R. (2017). Advantages of cortical surface reconstruction using submillimeter 7 T MEMPRAGE. *NeuroImage*.

Zilles, K., & Amunts, K. (2015). Anatomical basis for functional specialization. In K. Uludag, K. Ugurbil, & L. Berliner (Eds.), *fMRI: From nuclear spins to brain functions* (pp. 27–66). Boston, MA: Springer US.

SUPPORTING INFORMATION

Additional Supporting Information may be found online in the supporting information tab for this article.

How to cite this article: Haast RAM, Ivanov D, Uludağ K. The impact of B_1^+ correction on MP2RAGE cortical T_1 and apparent cortical thickness at 7T. *Hum Brain Mapp*. 2018;39:2412–2425. https://doi.org/10.1002/hbm.24011